Low-rank approach for image nonblind deconvolution with variance estimation

Hang Yang
Guosheng Hu
Yuqing Wang
Xiaotian Wu

Low-rank approach for image nonblind deconvolution with variance estimation

Hang Yang,[a,*] Guosheng Hu,[b] Yuqing Wang,[a] and Xiaotian Wu[a]
[a]Changchun Institute of Optics, Fine Mechanics and Physics, Chinese Academy of Science, Dongnanhu Road, Changchun 130033, China
[b]INRIA Grenoble Rhône-Alpes, 655 avenue de l'Europe, 38330 Montbonnot, France

Abstract. We develop a low-rank approach for image restoration by exploiting the image's nonlocal self-similarity. We assume that the matrix stacked by the vectors of nonlocal similar patches is of low rank and has sparse singular values. Based on this assumption, we propose a new image deconvolution algorithm that decouples the deblurring and denoising steps. Specifically, in the deblurring step, we involve a regularized inversion of the blur in the Fourier domain, which amplifies and colors the noise and corrupts the image information. Hence, in the denoising step, a singular-value decomposition of similar packed patches is used to efficiently remove the colored noise. Furthermore, we derive an approach to update the estimation of noise variance for setting the threshold parameter at each iteration. Experimental results clearly show that the proposed algorithm outperforms many state-of-the-art deblurring algorithms such as iterative decoupled deblurring BM3D in terms of both improvement in signal-to-noise-ratio and visual perception quality. © 2015 SPIE and IS&T [DOI: 10.1117/1.JEI.24.6.063013]

Keywords: low rank; image deconvolution; variance estimation.

Paper 15574 received Jul. 17, 2015; accepted for publication Oct. 30, 2015; published online Dec. 9, 2015.

1 Introduction

Image deconvolution is a long-standing challenge existing in the field of image processing, including optical, astronomical, physical, and medical applications.

The degradation procedure is often modeled as the result of a convolution with a low-pass filter,

$$g = h * x_{\text{orig}} + \gamma, \tag{1}$$

where g and x_{orig} are the observed and original images, respectively. γ is generally assumed to be independent and identically distributed, and is sampled from a zero mean density of variance η^2. h is the point spread function (PSF) of a linear time-invariant system, and $*$ denotes the convolution operation.

There are two main classes of image deconvolution methods: one relies on a preprocessing step followed by denoising,[1–4] whereas the other is based on a variational optimization problem which minimizes a cost function composed of fidelity and penalty terms.[5–9] The ForWaRD,[1] shape-adaptive discrete cosine transform,[3] and block-matching and 3D filtering deblurring[4] are examples of the first category. They preserve the features like edges but suffer from ringing artifacts near edges. On the other hand, the total variance model,[10] L_0-analysis-based sparse (ABS),[11] nonlocally centralized sparse representation (NCSR),[12] and iterative decoupled deblurring BM3D (IDDBM3D)[9] belong to the second category. These methods are well known for their detail-preserving property. As far as we know, NCSR and IDDBM3D achieve the state-of-the-art image deblurring performance.

Due to the property of image nonlocal self-similarity, one can obtain many patches similar to a given one across the image. In this work, we can stack the vectors of these similar patches to a low-rank matrix and design denoising algorithms by approximating the low-rank matrix. We integrate the low-rank method into an iterative deconvolution method. The iterative process consists of two parts: deblurring and denoising. The output of the deblurring process is a sharp but noisy estimated image. During the denoising process, the low-rank matrix approximation method is applied to the output of the deblurring step to suppress the noise and artifacts. Furthermore, the noise variance plays an important role in our method. We update the estimation of noise variance to compute a threshold parameter in each iteration. Experiments manifest that the proposed algorithm outperforms many state-of-the-art schemes in both numerical and visual perception.

To our knowledge, IDDBM3D is a block-matching three-dimensional transform-based image deconvolution method, and NSCR is a dictionary learning-based restoration method, whereas our method is a singular-value decomposition (SVD)-based approach. There are two differences between the first two approaches and our: first, we use a decoupled iterative scheme with SVD shrinkage, which is different from IDDBM3D and NCSR. An efficient deblurring method based on a fast Fourier transform (FFT) can be used in the deblurring step and an effective SVD-based denoising method is used in the following step; the other two methods must obtain a dictionary for the image denoising in the iteration. Second, we estimate the variance of colored noise; it is useful to set the threshold for denoising, whereas the other two use a fixed threshold in the experiment.

1.1 Paper Organization

The remainder of this paper is organized as follows. Section 2 gives a brief overview of low rank. Section 3

---

*Address all correspondence to: Hang Yang, E-mail: yanghang09@mails.jlu.edu.cn

shows how the low rank is used for regularizing the deconvolution problem and how to estimate the variance of the leaked noise. Section 4 demonstrates the effectiveness of our approach via simulation. Section 5 provides concluding remarks.

2 Low-Rank Minimization

The low-rank matrix recovery problem aims to estimate a low-rank matrix X from its noisy observation matrix Y.[13–15] This is a nonconvex problem, and Cai et al.[14] proposed to solve it by convex relaxation with the following nuclear norm:

$$\hat{X} = \arg \min_{X} \|X\|_*, \quad \text{s.t.} \ \|Y - X\|_2^2 \leq \eta^2. \tag{2}$$

The $\|X\|_*$ denotes the nuclear norm of a matrix X. It is defined as the sum of X's singular values, that is, $\|X\|_* = \sum_i \sigma_i(X)$, where $\sigma_i(X)$ means the ith singular value of X.

In the SVD domain, the following method is used:

$$(U, \Sigma, V) = \arg \min_{U, \sum, V} \|Y - U\Sigma V\|_2^2 + \sum_i \sigma_i(X), \tag{3}$$

where U and V are the orthonormal matrices. In Ref. 14, the authors have proved that the optimal solution of the minimization problem [Eq. (3)] can be simply achieved by the singular soft-thresholding operation,

$$\begin{cases} (U, \Sigma, V) = \text{SVD}(Y) \\ \hat{\Sigma} = S_\tau(\Sigma) \end{cases}, \tag{4}$$

where S_τ denotes the soft-thresholding operator with threshold τ, and the reconstructed data matrix $\hat{X}$ is conveniently obtained by $\hat{X} = U\hat{\Sigma}V^T$.

Now, we explore a nonlocal self-similarity approach based on the SVD. Given a reference patch p from a noisy image, we select a group of patches in the image which are similar to p. The similarity is defined in Ref. 4. Let us consider that there are $\mathcal{N}(p)$ such similar patches (including p) which are labeled as j, where $1 \leq j \leq \mathcal{N}(p)$. Next, we stack these similar patch vectors to form a matrix $Y_p = [y_1, y_2, \ldots, y_j, \ldots, y_{|\mathcal{N}(p)|}]_{j \in \mathcal{N}(p)}$, which is a low-rank matrix and has sparse singular values. Therefore, the low-rank minimization method [Eq. (3)] can be used to design filtered algorithms.

3 Low-Rank-Based Image Deconvolution

3.1 Proposed Deconvolution Algorithm

Our algorithm is based on the decoupling of the deblurring and denoising steps in the restoration process: (1) a regularized inversion of the blur in the Fourier domain in the deblurring step and (2) a denoising step using a low-rank approach. We will describe these two steps in detail in this section.

In the deblurring step, we proposed the cost function as follows:

$$y^k = \arg \min_{y} \{\lambda^k \|y - x_E^k\|_2^2 + \|h * y - g\|_2^2\}, \tag{5}$$

where k is the current iteration number, x_E^k is a pre-estimated image, and $\lambda^k > 0$ is the weight for the regularization term.

Alternatively, we diagonalized derivative operators after FFT for speedup. These yield solutions in the Fourier domain:

$$\mathcal{F}(y^k) = \frac{\mathcal{F}(h)^* \cdot \mathcal{F}(g) + \lambda^k \mathcal{F}(x_E^k)}{|\mathcal{F}(h)|^2 + \lambda^k}, \tag{6}$$

where $\mathcal{F}$ is the FFT operator and $\mathcal{F}(\cdot)^*$ denotes the complex conjugate. The plus, multiplication, and division are all component-wise operators.

The deblurred image y^k depends greatly on the regularization weighting λ^k. In this work, the parameter λ^k (kth step) in Eq. (6) is obtained using the following method:

$$\lambda^0 = \frac{N^2 \eta^2}{\|g - E(g)\|_2^2 - N^2 \eta^2}, \tag{7}$$

$$\lambda^{k+1} = \beta \lambda^k, \tag{8}$$

where the image size is $N \times N$ and $E(g)$ denotes the mean of g.

The goal of deconvolution is to restore a sharper image. In the deblurring step, Eq. (6) has the negative side effect of introducing new artifacts. To suppress the amplified noise and artifacts introduced in Eq. (6), in the denoising step, we applied the low-rank minimization method to filter the estimated image y^k.

The low-rank approach has shown promising performance in the image denoising problem; hence, we integrate it into the deconvolution model in this work.

Algorithm 1 Low-rank-based image deconvolution algorithm.

Input: Blurry and noisy image g, noise variance η^2.

1: Initialize: pre-estimated image $x_E^0 = 0$

2: for $k = 1$: K do

3:　　Use x_E^{k-1} to obtain the noisy image y^k via Eq. (5).

4:　　Noise variance update: re-estimate η_k^2 from y^k via Eq. (20).

5:　　for each patch y_p in y^k do

6:　　　Find similar patch group Y_p

7:　　　SVD for each noisy data matrix Y_p: $(U_p, \Sigma_p, V_p) = \text{SVD}(Y_p)$

8:　　　Thresholds update: compute τ_p using Eq. (12).

9:　　　Get the estimation using singular value thresholding [Eq. (11)] with computed τ_p.

11:　　end for

12. Image update: obtain an improved image x^k by weighted averaging all patches, and set $x_E^k = x^k$.

13: end for

Output: Deblurred image x^K.

Fig. 1 Example for the output of the deblurring algorithm prior to denoising with Barbara (scenario 5). From left to right, top to bottom, the 1st iteration, 10th iteration, 22nd iteration, and 34th iteration.

For each local patch y_p (size: $b \times b$) from image y^k, we can search a group [number: $\mathcal{N}(p)$] of its nonlocal similar patches in the image (in practice, in a large-enough image area) by block matching. To accomplish this, we define the block distance as the l^2-norm of the difference between the two blocks,

$$d(y_p, \bar{y}_p) = \frac{1}{b^2} \|y_p - \bar{y}_p\|_2^2, \tag{9}$$

where $\bar{y}_p$ is an arbitrary block in the search neighborhood. We selected $\mathcal{N}(p)$ patches with a minimum block distance, and $\mathcal{N}(p)$ is fixed as 20 in this work.

By stacking these similar patches' vectors into a $b^2 \times \mathcal{N}(p)$ matrix, denoted by Y_p, we get $Y_p = X_p + \Gamma_p$, where X_p and Γ_p are the patch matrices of the clean image and noise, respectively.

Then, the singular values of the matrix formed by these patches are calculated by SVD. For the natural image, X_p should be a low-rank matrix; thus, we can use the low-rank matrix approximation [Eq. (11)] to estimate X_p from Y_p:

$$\widehat{X_p} = \arg \min_{X_p} \|X_p\|_*, \quad \text{s.t. } \|Y_p - X_p\|_2^2 \leq \eta^2. \tag{10}$$

The $\|X_p\|_*$ denotes the nuclear norm of a matrix X_p.

The optimal solution can be obtained by the singular soft-thresholding operation,

$$\begin{cases} (U_p, \Sigma_p, V_p) = \text{SVD}(Y_p) \\ \widehat{\Sigma_p} = S_{\tau_p}(\Sigma_p) \end{cases}, \tag{11}$$

where U_p and V_p are the orthonormal matrices. The reconstructed data matrix $\widehat{X_p}$ is obtained by $\widehat{X_p} = U_p \widehat{\Sigma_p} V_p^{\mathsf{T}}$.

Then the whole image can be recovered by aggregating all the denoised patches.[16] We integrated a low-rank minimization method into the deconvolution problem, leading to a powerful algorithm.

Table 1 Experimental settings with different blur kernels and different values of noise variance σ^2 for pixel values in [0,255].

Tests	Point spread function (PSF)	σ^2
1	$h(i,j) = 1/(1 + i^2 + j^2)$, for $i, j = -7, \ldots, 7$	2
2	$h(i,j) = 1/(1 + i^2 + j^2)$, for $i, j = -7, \ldots, 7$	8
3	h is a 9×9 uniform kernel (boxcar)	≈ 0.3
4	$h = [1\,4\,6\,4\,1]^{\mathsf{T}}[1\,4\,6\,4\,1]/256$	49
5	h is a 25×25 Gaussian PSF with standard deviation 1.6	4
6	h is a 25×25 Gaussian PSF with standard deviation 0.4	64

Table 2 Comparison of the output improvement in signal-to-noise-ratio [ISNR (dB)] of the proposed deblurring algorithm. Blurred signal-to-noise ratio (BSNR) is defined as BSNR $= 10 \log_{10} \text{Var}(g)/N^2\sigma^2$, where Var() is the variance.

	Scenario						Scenario					
	1	2	3	4	5	6	1	2	3	4	5	6
Method	Cameraman (256 × 256)						House (256 × 256)					
BSNR	31.87	25.85	40.00	18.53	29.19	17.76	29.16	23.14	40.00	15.99	26.61	15.15
TVS	7.41	5.24	8.56	2.57	3.36	1.37	7.98	6.57	10.39	4.49	4.72	2.44
L0-ABS	7.70	5.55	9.10	2.93	3.49	1.77	8.40	7.12	11.06	4.55	4.80	2.15
SURE-LET	7.54	5.22	7.84	2.67	3.27	2.45	8.71	6.90	10.72	4.35	4.26	4.38
IDDBM3D	8.85	**7.12**	10.45	3.98	4.31	**4.89**	9.95	8.55	12.89	5.79	5.74	**7.13**
NCSR	8.78	6.69	10.33	3.78	4.60	4.50	9.96	8.48	13.12	5.81	5.67	6.94
Our method	**8.90**	7.05	**10.70**	**3.99**	**4.62**	4.62	**10.09**	**8.67**	**13.49**	**6.03**	**6.22**	6.74

	Scenario						Scenario					
	1	2	3	4	5	6	1	2	3	4	5	6
Method	Lena (512 × 512)						Barbara (512 × 512)					
BSNR	29.89	23.87	40.00	16.47	27.18	15.52	30.81	24.79	40.00	17.35	28.07	16.59
TVS	6.36	4.98	7.87	3.52	3.61	2.79	3.10	1.33	3.49	0.63	0.75	0.59
L0-ABS	6.66	5.71	7.79	4.09	4.22	1.93	3.51	1.53	3.98	0.73	0.81	1.17
SURE-LET	7.71	5.88	7.96	4.42	4.25	4.37	4.35	2.24	6.02	1.13	1.06	1.20
IDDBM3D	7.97	6.61	8.91	4.97	4.85	**6.34**	7.64	3.96	6.05	1.88	1.16	5.45
NCSR	8.03	6.54	9.25	4.93	4.86	6.19	7.76	3.64	5.92	2.06	1.43	**5.50**
Our method	**8.25**	**6.78**	**9.31**	**5.13**	**5.08**	6.13	**8.31**	**5.17**	**6.95**	**2.34**	**1.70**	5.37

3.2 Variance Estimation of Deblurred Image

In the application of denoising, the larger the singular values are, the less energy should be shrunk. Obviously, the key issue now is the determination of threshold τ. With a spatially adaptive Laplacian prior, we can set the threshold parameter,[17]

$$\tau_p(i) = \frac{c\eta_k^2}{\sqrt{\max[\sigma_i(X_p)^2/\mathcal{N}(p) - \eta_k^2, 0] + 0.001}}, \quad (12)$$

where $c > 0$ is a constant, $\mathcal{N}(p)$ is the number of similar patches, and τ_p denotes the local threshold at position p.

In this work, we present an algorithm to update the estimation of noise variance η_k^2 at each iteration.

In Eq. (5), we can see that the noise of the image y^{k+1} is contained by two parts: $\gamma_{k+1,1}$ and $\gamma_{k+1,2}$. $\gamma_{k+1,1}$ is the feedback of regularized noise from g, and $\gamma_{k+1,2}$ is the leaked noise in the image $x_E^k = x_{\text{orig}} + \gamma^k$. From Eq. (6), one can find that

$$\mathcal{F}(y^{k+1}) = \mathcal{F}(x_{\text{orig}}^{k+1}) + \mathcal{F}(\gamma_{k+1,1}) + \mathcal{F}(\gamma_{k+1,2}), \quad (13)$$

where

$$x_{\text{orig}}^{k+1} = \mathcal{F}^{-1}\left(\frac{|\mathcal{F}(h)|^2 \cdot \mathcal{F}(x_{\text{orig}}) + \lambda^k \mathcal{F}(x_{\text{orig}})}{|\mathcal{F}(h)|^2 + \lambda^k}\right), \quad (14)$$

$$\gamma_{k+1,1} = \mathcal{F}^{-1}\left(\frac{\mathcal{F}(h)^* \cdot \mathcal{F}(\gamma)}{|\mathcal{F}(h)|^2 + \lambda^k}\right), \quad (15)$$

$$\gamma_{k+1,2} = \mathcal{F}^{-1}\left(\frac{\lambda^k \mathcal{F}(\gamma^k)}{|\mathcal{F}(h)|^2 + \lambda^k}\right). \quad (16)$$

Then we can compute the variance of $\gamma_{k+1,1}$ as

$$\eta_{k+1,1}^2 = E(| < \gamma_{k+1,1}, \gamma_{k+1,1} > |^2) \quad = \eta^2 \left\| \frac{\mathcal{F}(h)^*}{|\mathcal{F}(h)|^2 + \lambda^k} \right\|^2. \quad (17)$$
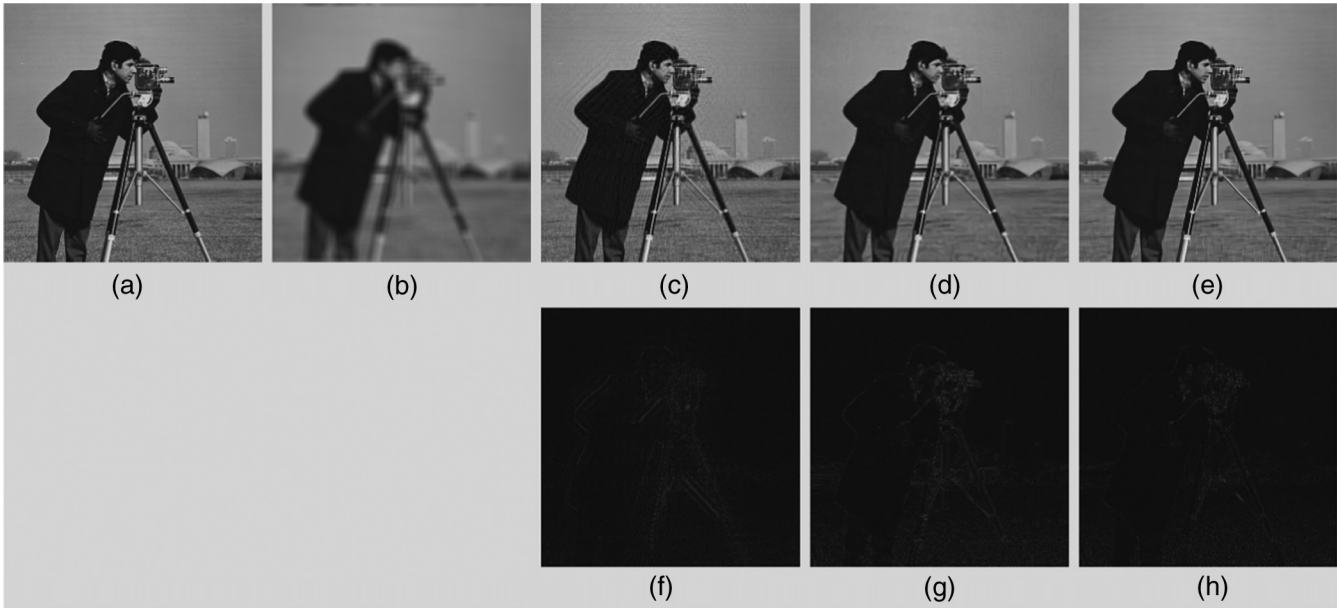
Fig. 2 Visual quality comparison of image deblurring on gray cameraman image. (a) Original image, (b) noisy and blurred image (scenario 3), (c) NCSR [improvement in signal-to-noise-ratio (ISNR) = 10.33 dB], (d) iterative decoupled deblurring BM3D (IDDBM3D) (ISNR = 10.45 dB), (e) our method (ISNR = 10.70 dB), (f) difference image between the ground truth and nonlocally centralized sparse representation (NCSR) results, (g) difference image between the ground truth and the IDDBM3D results, and (h) difference image between the ground truth and our results.
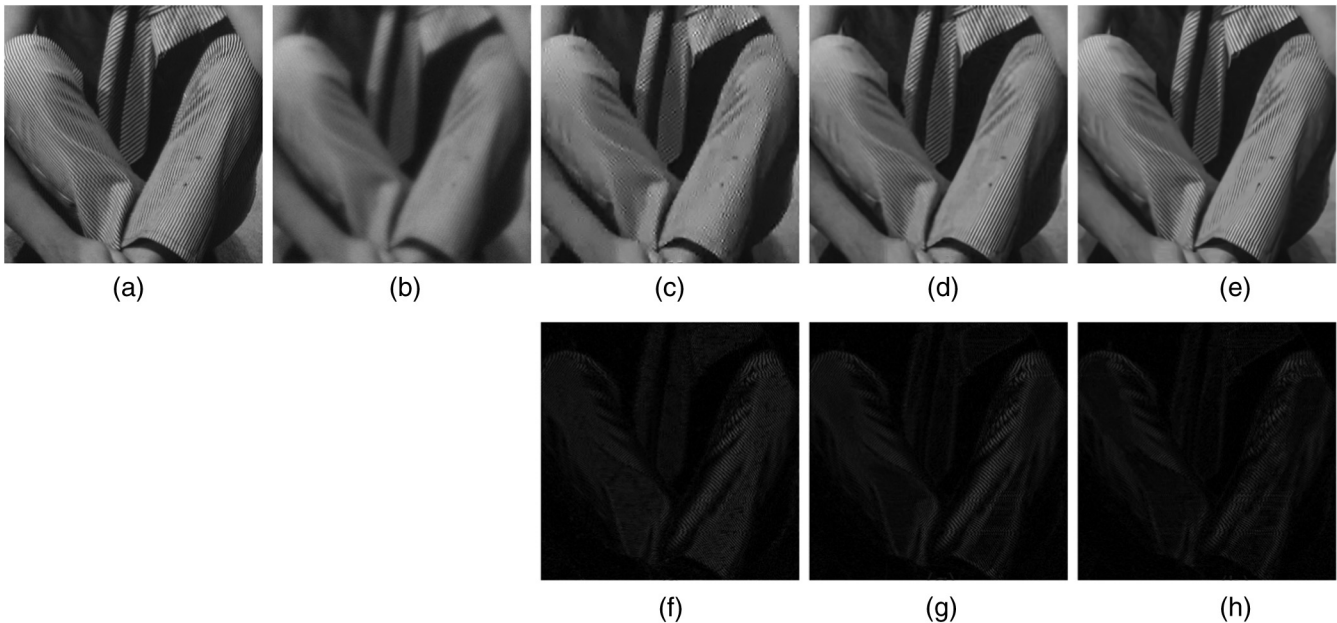
Fig. 3 Details of the image deconvolution experiment on image Barbara. (a) Original image, (b) noisy and blurred image (scenario 2), (c) SURE-LET (ISNR = 2.24 dB), (d) IDDBM3D (ISNR = 3.96 dB), (e) our method (ISNR = 5.17 dB), (f) difference image between the ground truth and the SURE-LET results, (g) difference image between the ground truth and the IDDBM3D results, and (h) difference image between the ground truth and our results.

Similar to $\gamma_{k+1,1}$, we can estimate the variance of leaked noise $\gamma_{k+1,2}$ in the denoised image x^k as

$$\eta_{k+1,2}^2 = \text{Var}(\gamma^k)\|\frac{\lambda^k}{|\mathcal{F}(h)|^2 + \lambda^k}\|^2, \tag{18}$$

$$\text{Var}(\gamma^k) = c_0(\eta_k^2 - \|y^k - x^k\|_2^2), \tag{19}$$

where η_k^2 is the noise variance of y^k, $\text{Var}()$ denotes the variance, $\|y^k - x^k\|_2^2$ is the variance of the removed noise, and $c_0 > 0$ is a scaling factor controlling the re-estimation of the noise variance.

Finally, the noise variance of y^{k+1} is updated as

$$\eta_{k+1} = c_1 \sqrt{\eta_{k+1,1}^2 + \eta_{k+1,2}^2}, \tag{20}$$
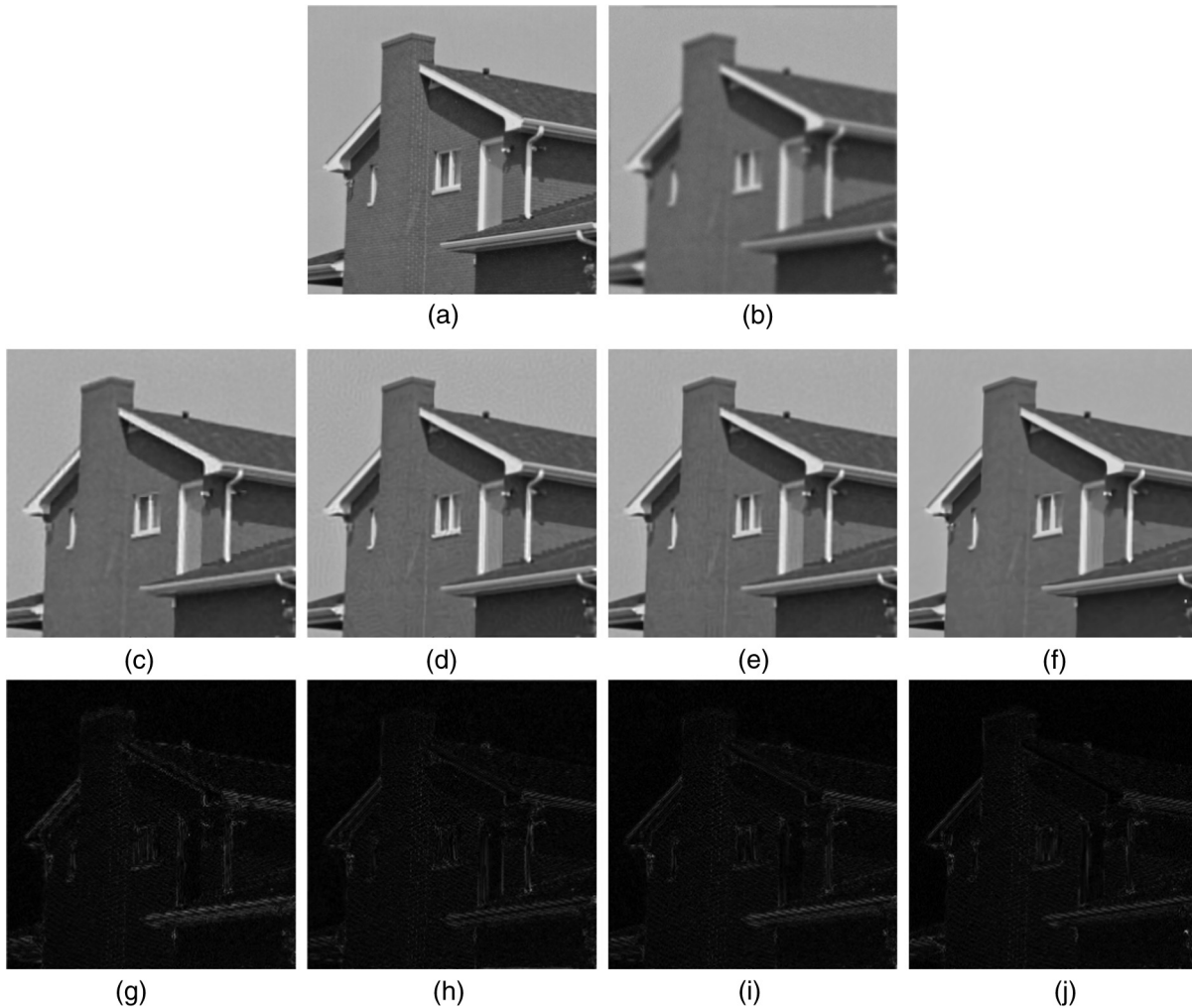
Fig. 4 Visual quality comparison of image deblurring on house image. (a) Original image, (b) noisy and blurred image (scenario 5), (c) L0-analysis-based sparse (ABS) (ISNR = 4.80 dB), (d) NCSR (ISNR = 5.67 dB), (e) IDDBM3D (ISNR = 5.74 dB), (f) our method (ISNR = 6.22 dB), (g) difference image between the ground truth and the L0-ABS results, (h) difference image between the ground truth and the NCSR results, (i) difference image between the ground truth and the IDDBM3D results, and (j) difference image between the ground truth and our results.

where $c_1 > 0$ is a scale factor. In Eqs. (12) and (13), we can see that the two noises, $\gamma_{k,1}$ and $\gamma_{k,2}$, are not independent to each other, so we use c_1 to control the estimation of noise variance.

Equation (20) can be described as follows: when the iteration starts, only strong image details can be retained after soft-thresholding shrinkage and contribute to the initial estimation of x; however, the partially recovered image will be fed back to the blurred and noisy observation through Eq. (5), which helps to reduce noise.[18] In return, weaker image details can be identified and added to the image estimate. As the iteration progresses, we observe that the estimated noise variance monotonically decreases; meanwhile, image details are progressively recovered.

The whole deconvolution algorithm is summarized in Algorithm 1.

4 Experimental Results

In all the simulations, we set $\beta = 1.25$ in Eq. (8). The choices of c_0 in Eq. (14) and c_1 in Eq. (20) are largely heuristic in nature. We have empirically found that $c_0 \in [0.3, 0.5]$ and

$c_1 \in [1.1, 1.4]$ generally yield good results and have accordingly set $c_0 = 0.4$ and $c_1 = 1.25$, respectively. We have found that the improvement in signal-to-noise-ratio (ISNR) generally reaches the peak value when $c \in [1.05, 1.55]$. We fix this parameter value to 1.2 in our experiments.

In our experiments, we set the size of the patch as 4×4 (i. e., $b = 4$), and we selected the first reference patch from the top left of image and used step 3 in both rows and columns to go from one reference patch to the next. For a 256×256 image, 84×84 patches are used for processing.

All the experiments are performed in MATLAB 7.11.0 on an Intel(R) Core CPU i75600U processor (2.60 GHz), 8.0 GB memory, and Windows 7 operating system (notebook PC). To estimate the complexity of our method, for an $N \times N$ image, we assume that the average time to compute similar patches for each reference patch is T. The SVD of each group with a size of $B \times c$ is $O(B \times c^2)$. The FFT costs $O(N^2 \log N)$ for the iterative update on deblurring and denoising. Hence, the total complexity for image deconvolution is $O[N^2(B \times c^2 + T + \log N)]$. For a 256×256 image, the proposed algorithm requires about 3.55 s for
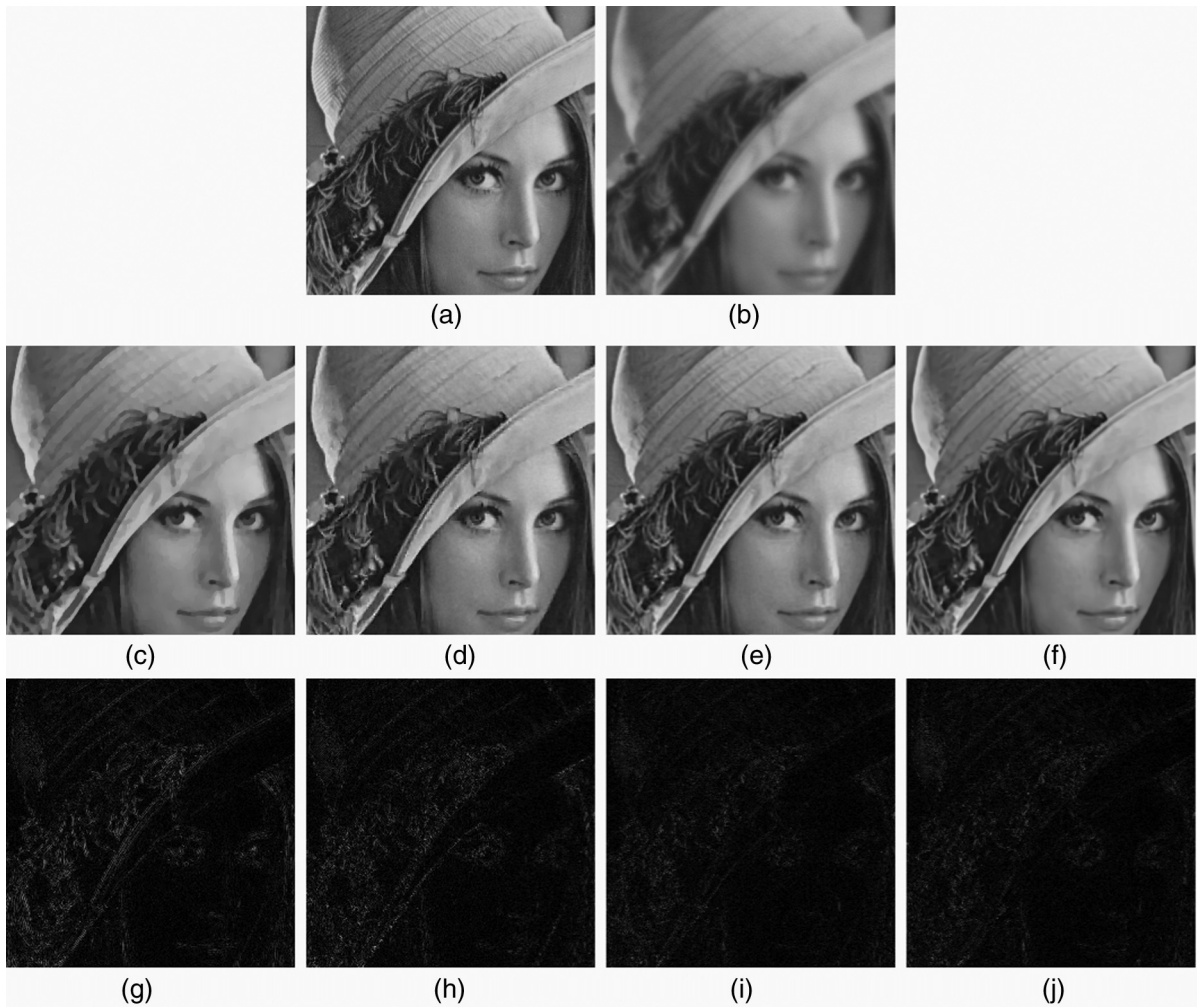
Fig. 5 Details of the image deconvolution experiment on Lena image. (a) Original image, (b) noisy and blurred image (scenario 1), (c) TVS (ISNR = 6.36 dB), (d) L0-ABS (ISNR = 6.66 dB), (e) IDDBM3D (ISNR = 7.97 dB), (f) our method (ISNR = 8.25 dB), (g) difference image between the ground truth and the TVS results, (h) difference image between the ground truth and the L0-ABS results, (i) difference image between the ground truth and the IDDBM3D results, and (j) difference image between the ground truth and our results.
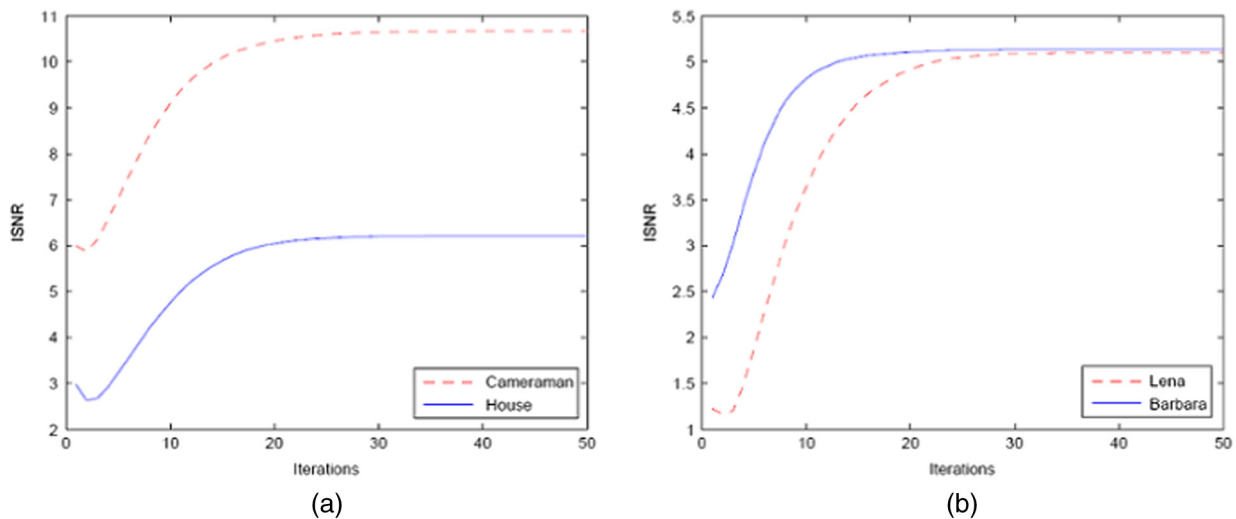

Fig. 6 Change of the ISNR with iterations for the different setups of the proposed algorithm. (a) Scenario 3 for cameraman, and Scenario 5 for house, (b) Scenario 4 for Lena, and Scenario 2 for Barbara.

Fig. 7 Test images.[21] From left to right, top to bottom: Img1, Img2, Img3, and Img4.

Fig. 8 Blur kernels.[21] From left to right, top to bottom: PSF1, PSF2, PSF3, and PSF4.

one iteration, where the time for searching similar patches requires about 2.12 s, and it is observed that about 35 iterations are typically sufficient. We have posted code online.[19]

In Fig. 1, we show an example for the output of the deblurring algorithm prior to denoising.

4.1 Benchmark Problems

The standard images cameraman, house, Lena, and Barbara are tested in our experiments. The experimental settings are presented in Table 1. Table 1 describes the different PSF and different amounts of white Gaussian additive noise. They are used in other papers[4,11] and go from weak-blur/strong-noise to strong-blur/weak-noise cases.

We compare the proposed method with four state-of-the-art algorithms: TVS,[10] L0-AbS,[11] SURE-LET,[20] NCSR,[12] and IDDBM3D[9] in standard test settings for deconvolution.

Table 3 Experimental settings with different blur kernels and different levels of noise.

Tests	Images	PSFs	BSNRs
1	Img1	PSF1	15
2	Img1	PSF2	20
3	Img2	PSF3	15
4	Img2	PSF4	20
5	Img3	PSF2	15
6	Img3	PSF1	20
7	Img4	PSF4	15
8	Img4	PSF3	20

Table 4 Comparison of the output ISNR (dB) of the proposed deblurring algorithm.

Methods	1	2	3	4	5	6	7	8
IDDBM3D	6.04	7.56	5.42	11.33	7.13	8.65	7.19	8.56
FHLD	5.05	6.92	4.82	10.47	5.54	6.45	7.69	5.71
DFD	4.35	6.27	4.10	8.76	5.59	4.54	10.43	6.47
Ours	**6.37**	**8.45**	**6.47**	**12.25**	**8.62**	**9.73**	**12.25**	**9.72**

Table 2 lists the comparison of ISNR results for six typical deblurring experiments. The highest ISNR results in the experiments are labeled in bold. The ISNR is defined as

$$\text{ISNR} = 10 \log_{10}\left(\frac{\|u_{\text{orig}} - y\|_2^2}{\|u_{\text{orig}} - \hat{u}\|_2^2} \right), \tag{21}$$

where $\hat{u}$ is the corresponding estimated image. It is clear that our algorithm achieves the highest ISNR results in most cases, as labeled in bold. In particular, for image Barbara(512×512) with rich textures, our method outperforms current state-of-the-art methods, NCSR and IDDBM3D, by more than 0.9 dB in scenarios 2 and 3.

The visual comparisons of the deblurring methods are shown in Figs. 2 and 3, from which one can observe that the proposed method produces cleaner and sharper image edges and textures than other competing methods. Figure 2 shows that our result [Fig. 2(e)] is more visually pleasant than those in Figs. 2(c) and 2(d). In Fig. 3, our result [Fig. 3(e)] preserves most details on Barbara's trousers.

We provided more visual comparisons in Figs. 4 and 5. Here, we provided empirical evidence to illustrate the stability of the proposed deconvolution method. Figure 6 plots the evolutions of ISNR versus iteration numbers for test images in the cases of scenario 3 for cameraman, scenario 5 for house, scenario 4 for Lena, and scenario 2 for Barbara. It is observed that with the growth of iteration number, all the ISNR curves increase monotonically and ultimately become flat and stable, exhibiting good stability of the proposed
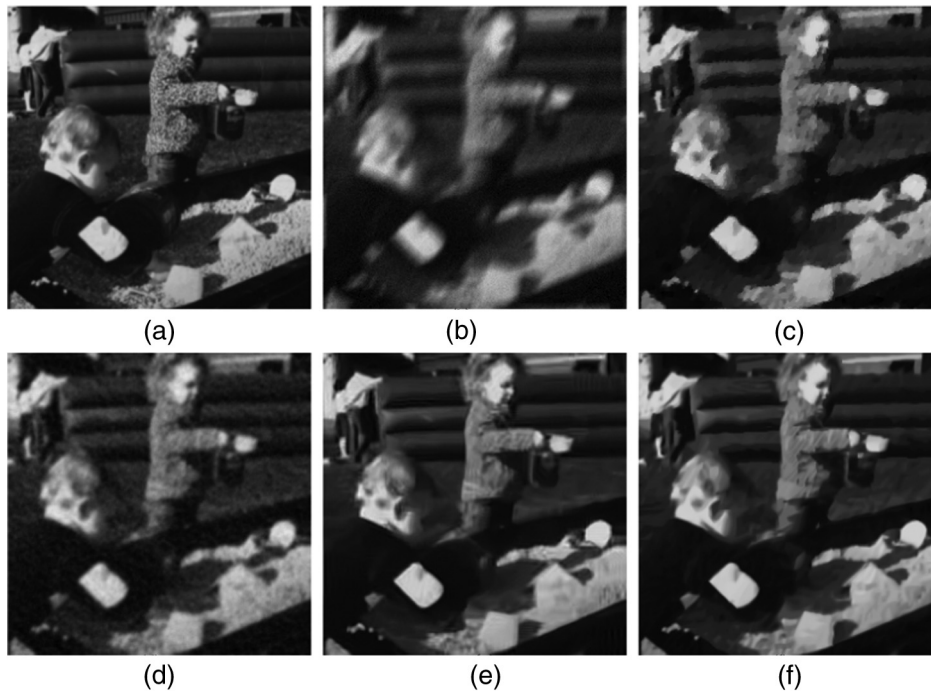
(a) (b) (c)

(d) (e) (f)

Fig. 9 Example of the deconvolution results with Img1 image in experiment 2. (a) Original image, (b) noisy and blurred image (scenario 5), (c) fast hyper-Laplacian based deconvolution (FHLD) (ISNR = 6.92 dB), (d) directional filters based deconvolution (DFD) (ISNR = 6.27 dB), (e) IDDBM3D (ISNR = 5.42 dB), and (f) our method (ISNR = 8.45 dB).

model. One can also observe that 35 iterations are typically sufficient.

4.2 More Complicated Point Spread Function

we provide simulations with more images (shown in Fig. 7) and blur kernels (shown in Fig.8) database used in Ref. 21.

We compare the proposed method with four state-of-the-art algorithms: IDDBM3D,[9] fast hyper-Laplacian based deconvolution (FHLD),[22] and directional filters based deconvolution (DFD)[23] in the test settings for deconvolution. The results for IDDBM3D, FHLD, and DFD are obtained using the software available online. We use the default parameters
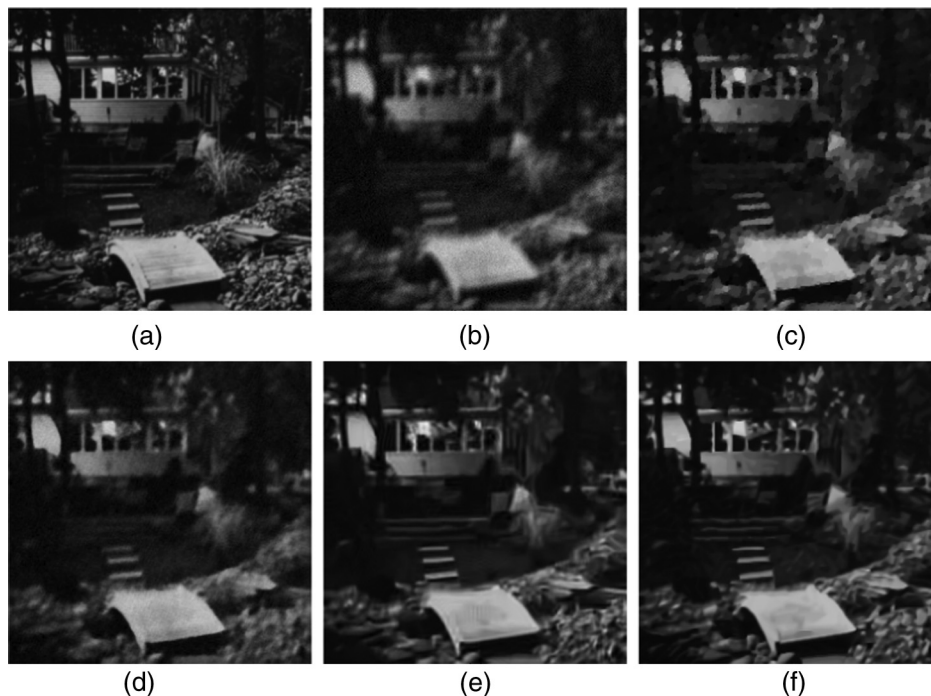

(a) (b) (c)

(d) (e) (f)

Fig. 10 Visual quality comparison of the results with Img2 image in experiment 3. (a) Original image, (b) noisy and blurred image (scenario 5), (c) FHLD (ISNR = 4.82 dB), (d) DFD (ISNR = 4.10 dB), (e) IDDBM3D (ISNR = 7.56 dB), and (f) our method (ISNR = 6.47 dB).
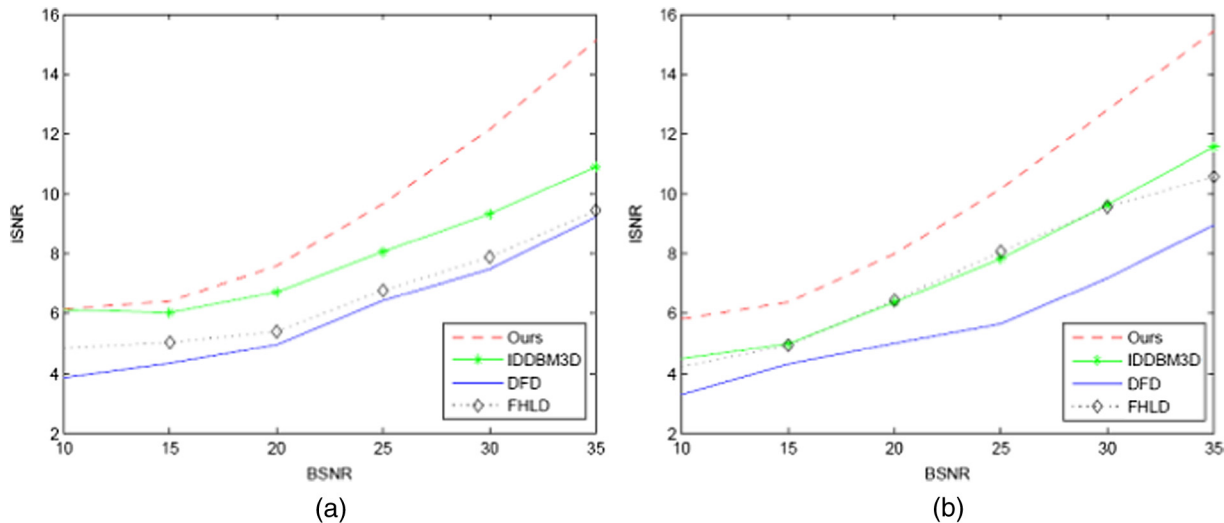
Fig. 11 Algorithm's sensitivity to different levels of noise. (a) The test image is Img1 and the blur kernel is PSF1, (b) the test image is Img2 and the blur kernel is PSF2.

suggested by the authors of the algorithms. The experiment settings are presented in Table 3. The comparison of ISNR results is listed in Table 4. The highest ISNR results in the experiments are labeled in bold.

The visual comparisons of the deblurring methods are shown in Figs. 9 and 10. One can see that our results are more visually pleasant than the others. Results have shown that the proposed method obtains a deblurring result with better quantitative and visual performance.

We provide the algorithm's sensitivity to different levels of noise with the same blur kernel and latent sharp image in Fig. 11. The test images are Img1 and Img2. PSF1 and PSF2 are used in the experiments, respectively. To each blurred image, Gaussian noise is added such that the blurred signal-to-noise ratios (BSNRs) of the observed images are 10, 15, 20, 25, 30, and 35 dB. From Fig. 11, we can find that the ISNR values are monotonically increasing on BSNR.

5 Conclusion

A low-rank (SVD-based) approach which models nonlocal similarity in images was proposed, leading to a conceptually simple image deconvolution algorithm with the decoupling of the deblurring and denoising steps. We also proposed a simple and effective method of estimating the noise variance via computing the thresholds in each iteration. The experimental results showed that our algorithm can not only lead to visible ISNR improvements over state-of-the-art methods, such as IDDBM3D and NCSR but also much better preserve the image local structures and greatly reduce visual artifacts.

References

1. R. Neelamani, H. Choi, and R. G. Baraniuk, "ForWaRD: Fourier-wavelet regularized deconvolution for ill-conditioned systems," *IEEE Trans. Image Process.* **52**, 418–433 (2004).
2. H. Yang and Z. B. Zhang, "Fusion of wave atom-based Wiener shrinkage filter and joint non-local means filter for texture-preserving image deconvolution," *Opt. Eng.* **51**, 067009 (2012).
3. A. Foi et al., "Shape-adaptive DCT for denoising and image reconstruction," *Proc. SPIE* **6064**, 60640N (2006).
4. K. Dabove et al., "Image restoration by sparse 3D transform-domain collaborative filtering," *Proc. SPIE* **6812**, 681207 (2008).
5. H. Yang, M. Zhu, and X. Wu, "Dictionary learning approach for image deconvolution with variance estimation," *Appl. Opt.* **53**(24), 5677–5683 (2014).
6. H. Huang, H. Yang, and S. Ma, "Gradient-based image deconvolution," *J. Electron. Imaging* **22**(1), 013006 (2013).
7. Y. Wang et al., "A new alternating minimization algorithm for total variation image reconstruction," *SIAM J. Imaging Sci.* **1**, 248–272 (2008).
8. H. Yang et al., "Edge-preserving image deconvolution with nonlocal domain transform," *Opt. Laser Technol.* **54**, 128–136 (2013).
9. A. Danielyan, V. Katkovnik, and K. Egiazarian, "BM3D frames and variational image deblurring," *IEEE Trans. Image Process.* **21**(4), 1715–1728 (2012).
10. O. V. Michailovich, "An iterative shrinkage approach to total-variation image restoration," *IEEE Trans. Image Process.* **20**, 1281–1299 (2011).
11. J. Portilla, "Image restoration through l_0 analysis-based sparse optimization in tight frames," in *Proc. 16th IEEE ICIP*, Cairo, Egypt, pp. 3909–3912 (2009).
12. W. Dong et al., "Nonlocally centralized sparse representation for image restoration," *IEEE Trans. Image Process.* **22**(4), 1620–1630 (2013).
13. E. Candes and Y. Plan, "Matrix completion with noise," *Proc. IEEE* **98**(6), 925–936 (2010).
14. J. Cai, E. Candes, and Z. Shen, "A singular value thresholding algorithm for matrix completion," *SIAM J. Optim.* **20**, 1956–1982 (2010).
15. H. Ji et al., "Robust video restoration by joint sparse and low rank matrix approximation," *SIAM J. Imaging Sci.* **4**(4), 1122–1142 (2011).
16. S. H. Gu et al., "Weighted nuclear norm minimization with application to image denoising," in *Proc. 27th IEEE Conf. on Computer Vision and Pattern Recognition (CVPR)*, pp. 2862–2869 (2014).
17. S. G. Chang, B. Yu, and M. Vetterli, "Adaptive wavelet thresholding for image denoising and compression," *IEEE Trans. Image Process.* **9**(9), 1532–1546 (2000).
18. W. Dong, G. Shi, and X. Li, "Nonlocal image restoration with bilateral variance estimation: a low-rank approach," *IEEE Trans. Image Process.* **22**(2), 700–711 (2013).
19. H. Yang et al., "Deblurring low rank," https://cn.mathworks.com/matlabcentral/fileexchange/53678-deblurring-low-rank (26 Oct 2015).
20. F. Xue, F. Luisier, and T. Blu, "Multi-Wiener SURE-LET deconvolution," *IEEE Trans. Image Process.* **22**(5), 1954–1968 (2013).
21. A. Levin et al., "Understanding and evaluating blind deconvolution algorithms," in *Proc. 22th IEEE Conf. on Computer Vision and Pattern Recognition (CVPR)*, pp. 1964–1971 (2009).
22. D. Krishnan et al., "Fast image deconvolution using hyper-Laplacian priors," in *Advances in Neural Information Processing Systems (NIPS)*, pp. 1033–1041 (2009).
23. L. Zhong et al., "Handling noise in single image deblurring using directional filters," in *Proc. 26th IEEE Computer Vision and Pattern Recognition (CVPR)*, pp. 612–619 (2013).

Hang Yang is an assistant researcher at the Changchun Institute of Optics, Fine Mechanics, and Physics, Chinese Academy of Science.

He received his BS and PhD degrees in mathematics from Jilin University in 2007 and 2012, respectively. His current research interests include image deconvolution, image motion deblurring, and image fusion.

Guosheng Hu is a postdoctoral researcher at the INRIA Grenoble, France. He received his MS degree in computer sciences from Jilin University, China, in 2010 and his PhD in computer sciences from Surary University, UK, in 2015. His current research interests include face recognition and deep learning.

Yuqing Wang is an associate researcher at the Changchun Institute of Optics, Fine Mechanics, and Physics, Chinese Academy of Science. He received his PhD in electrical engineering from Changchun

Institute of Optics, Fine Mechanics, and Physics, Chinese Academy of Science, in 2009. His current research interests include image enhancement, image quality metrics, and image fusion.

Xiaotian Wu is an assistant researcher at the Changchun Institute of Optics, Fine Mechanics, and Physics, Chinese Academy of Science. He received his BS degree in electrical engineering from Jilin University in 2009 and his MS degree in electrical engineering from Xiamen University in 2012. His current research interests include image dehazing and image compression.